DOI: 10.1111/mice.12507

ORIGINAL ARTICLE

COMPUTER-AIDED CIVIL AND INFRASTRUCTURE ENGINEERING WILEY

Behavioral decision-making model of the intelligent vehicle based on driving risk assessment

Xunjia Zheng[1] | **Heye Huang**[1] | **Jianqiang Wang**[1] | **Xiaocong Zhao**[2] | **Qing Xu**[1]

[1]The State Key Laboratory of Automotive Safety and Energy, Tsinghua University, Beijing, China

[2]School of Automobile and Traffic Engineering, Jiangsu University, Zhenjiang, China

Correspondence
Jianqiang Wang, The State Key Laboratory of Automotive Safety and Energy, Tsinghua University, Beijing 100084, China.
Email: wjqlws@tsinghua.edu.cn

Assistant Professor Qing Xu is a co-corresponding author of this article.

Funding information
National Science Fund for Distinguished Young Scholars, Grant/Award Number: 51625503; National Natural Science Foundation of China, Grant/Award Number: 61790561

Abstract

Intelligent-driving technologies play crucial roles in reducing road-traffic accidents and ensuring more convenience while driving. One of the significant challenges in developing an intelligent vehicle is how to operate it safely without causing fear in other human drivers. This paper presents a new behavioral decision-making model to achieve both safety and high efficiency and also to reduce the adverse effect of autonomous vehicles on the other road users while driving. Moreover, we attempt to adapt the model for human drivers so that users can understand, adapt, and utilize intelligent-driving technologies. Furthermore, this paper proposes a combined spring model for assessing driving risk. Thus, we analyze some driving characteristics of drivers and choose "safety" and "high efficiency" as the two main factors that are pursued by drivers while driving. Based on the principle of least action, a multiobjective optimization cost function is established for the decision-making model. Finally, we design six unprotected left-turn scenarios at a T-intersection and three unprotected left-turn scenarios at a standard two-lane intersection for applying simulation algorithm and provide a decision-making map for developing intelligent-driving technologies. Based on the principle of least action, this paper demonstrates that optimization theory can give insight into drivers' behavior and can also contribute to the development of intelligent-driving algorithms. The experimental results reveal that the behavioral decision-making model can always avoid collision accidents on the premise of ensuring certain efficiency, and it can achieve 97.01%, 94.52%, 96.67%, 91.18%, 101.27%, 83.33%, 102.94%, 103.03%, and 105.77% of time to intersection's maximum pass rate in the considered nine scenarios.

1 | INTRODUCTION

Intelligent vehicles, such as vehicles equipped with advanced driver assistant systems, have played significant roles in driving to reduce the number of accidents, enhance safety, improve efficiency, and provide convenience to drivers while driving. They are supposed to adapt to human drivers' behaviors when introduced into the contemporary traffic system, rather than being too cautious or too careful. Hence, decision-making algorithms form a fundamental critical component for intelligent vehicles autonomy. When intelligent vehicles are transporting passengers or goods from a given place to another, they need to consider a strategy that incorporates searching for the shortest possible distance to follow; which avoids obstacles and generates the best trajectory that ensures safety, comfort, and efficiency (Gu & Dolan, 2014).

Significant progress has been achieved in intelligent vehicles autonomy by applying decision-making algorithms. Most of the existing decision-making algorithms originate from the field of robotics, and they have been subsequently applied to vehicles' transportation. Google and Stanford teams have conducted some preliminary researches on how to learn from excellent drivers' driving behaviors for intelligent vehicles' decision making. For example, studies have been conducted on driving decision-making pattern transfer model (Okuda, Ikami, Suzuki, Tazaki, & Takeda, 2013) and on driving decision-making gray relational analysis and entropy (Teichman, Lussier, & Thrun, 2013). Some researchers have also employed iterative dichotomiser 3 (ID3) classification algorithm in decision making based on real-time local elevation map (Hoult & Cole, 2008). The feasible direction algorithm and vector field histogram have also been applied to the motion planning of autonomous vehicles (Wei, Snider, Gu, Dolan, & Litkouhi, 2014). Based on various driving strategy search methods and decision-making behaviors, the decision-making methods for intelligent vehicles can be classified into four categories (Jo, Kim, Kim, Jang, & Sunwoo, 2015): state machine model, knowledge-based reasoning decision-making model, decision/behavior tree model, and utility/value-based decision model. Although these traditional decision-making models have yielded excellent results in the realization of intelligent vehicles with human driving behavior, they have limitations when applied to intelligent vehicles in some areas (Zhu & Ukkusuri, 2018). Most of the aforementioned behavioral decision-making methods obtain their driving strategies from previous knowledge using heuristic methods. Moreover, it is necessary to specify or adopt a set of driving strategies for each driving scene, which makes it difficult to achieve decision making in intelligent vehicles autonomy that is indeed adapted to human drivers' behavior; it not only plays the role of the driver in the subject vehicle, but also considers the other human drivers.

Deep learning methods have also been applied to the study of behavioral decision-making system of intelligent vehicles recently. For simulating a human driver's behavior to achieve the autonomous driving of an unmanned vehicle, some researchers employed convolutional neural network learning from the perspective of pixel-level image characteristics to the mapping relationship between the specific control instructions (Bojarski et al., 2016). Furthermore, some other researchers have applied similar approaches (e.g., Mohanan & Salgoankar, 2018). To design the vehicle behavior decision-making algorithm, probabilistic process, game-theoretic process, and Markov decision process have been introduced (Nolte, Ernst, Richelmann, & Maurer, 2018). These algorithms can consider other drivers' intention and integrate them into the decision-making algorithm to achieve collaborative decision making. Moreover, these methods depend mostly on the information reception of some expensive sensors and require a substantial amount of accurate data; moreover, they suffer from poor interpretability.

From the above discussion, it is evident that previous researches have demonstrated technological feasibility to achieve intelligent vehicle autonomy. Currently, automobile companies and technology giants are accelerating the development of intelligent-driving research; although some existing intelligent vehicles have encountered several avoidable accidents during road-testing. Therefore, it is necessary that behavioral decision-making and control methods should explore the intellective ability of intelligent vehicle improvement.

In general, drivers have different goals while driving, such as arriving at their destination as soon as possible, avoiding an accident, and avoiding traffic violation. Most of the existing methods of multiobjective decision making are often task driven; besides most recent researches focus mainly on how to control the vehicle more safely, efficiently, smoothly, and economically while driving (Z. Wang, Chen, Ouyang, & Li, 2015). Dovgan, Javorski, Tušar, Gams, and Filipič (2014) designed a two-level multiobjective optimization algorithm and obtained a set of nondominated driving strategies by considering two conflicting objectives: the traveling time and fuel consumption. Subsequently, some researchers proposed a series of cogitative decision-making algorithms by considering the driving experience of the driver to enable intelligent vehicles to adopt human driver characteristics. Li, Li, Rajamani, and Wang (2011) presented a multiobjective decision-making algorithm, which comprehensively addressed the challenges of tracking capability, fuel economy, and driver's desired response. The authors designed the logic of the algorithm by combining several objectives into a weighted-sum cost function. Consequently, this will lead to mutual independence among various objectives that will not accurately reflect the driving decision-making process of the driver.

Recently, self-driving vehicles, such as the prototype vehicle of Waymo and Uber, have caused some traffic accidents. Besides, they interfere with other vehicles by creating unusual moves in some scenarios, such as a T-intersection, which nearly caused rear-end collisions in a particular scenario. Waymo prototypes often throw human drivers off guard with some driving behaviors, which shows that it has not reached the highest level of intelligence; moreover, it rarely imitates the behaviors of human drivers. The performance is because of the difficulty of intelligent vehicles to adopt the same risk perception and cognitive ability as human drivers in their decision-making process. Furthermore, it is crucial to organically integrate the multiple goals pursued by human drivers while driving.

Based on the assessment of the current risk situation, drivers often make decisions while driving. Furthermore, the driver perceives risk and makes decisions not only based on

the speed and position of other vehicles, but also the type of other vehicles. Hence, assessing the driving risk is the premise of behavioral decision making for intelligent vehicles. Herein, we introduce a new idea of decision making for intelligent vehicles from an overall perspective based on the driving risk assessment.

The rest of this paper is organized as follows. In Section 2, we discuss a whole framework to illustrate the overview of this study. Section 3 studies the generation and evolution rules of the driving risks from the perspective of drivers by identifying the major sources of driving risks. Section 4 considers "safety" and "high efficiency" as the main objectives of drivers while driving. It also presents the physical model of the driving process and the multiobjective decision-making model based on the principle of least action from a systematic and holistic perspective. In Section 5, we design six typical scenarios for verifying the simulation experiments and obtained possible trajectories based on various conditions using the calculations of simulation experiments. Section 6 conducts applications in three other conflict scenarios at standard intersections to verify the effectiveness of the proposed algorithm. Section 7 presents the discussions of this study, while Section 8 concludes the study.

2 | THEORETICAL FRAMEWORK

The theoretical architecture of behavioral decision making comprises three parts: vehicle interaction modeling, behavioral decision-making module, and an intelligent vehicle controller, as shown in Figure 1. Specifically, through sensors and other devices, traffic information, including vehicle, road, and environment, is obtained as input data of the risk evaluation module. Further, behavioral decision-making modeling is considered as a process of incorporating the principle of least action to establish a multiobjective decision-making model.

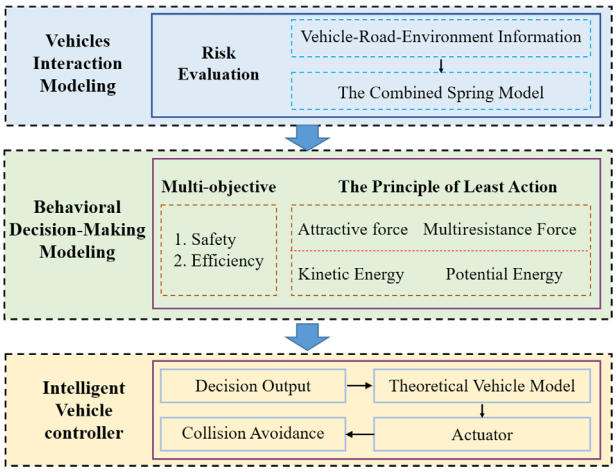

FIGURE 1 Overview of the behavioral decision-making model for intelligent vehicle

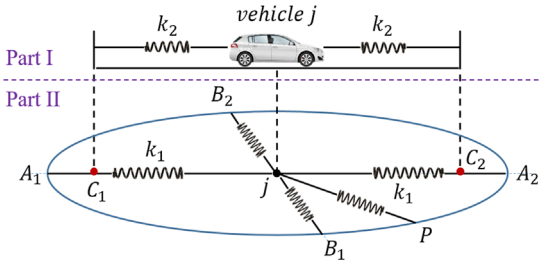

FIGURE 2 Skeleton of the combined spring model

Finally, the output-controlled variables are sent to the intelligent vehicle controller for executing collision avoidance. This study focuses on vehicle interactions and behavioral decision-making modules to improve intelligent vehicle technologies. We discuss the details of each submodule in the following subsections.

2.1 | Vehicle interaction and risk evaluation

This study presents a combined spring model to describe the interaction of vehicles and assess driving safety. Figure 2 depicts the combined spring model, which includes a multispring model with elliptic distribution and a spring oscillator model inserted between the ellipse foci. The spring model can vividly describe drivers' perception of risk (Raksincharoensak, Akamatsu, Moro, & Nagai, 2014). Furthermore, the visual characteristics of drivers are related closely to safe driving based on the main information acquisition channels in the traffic system. Moreover, visual discrimination ability is considerably affected while driving, and the visual field angle becomes narrow as the speed increases. Therefore, the driver's field of vision can be considered as an ellipse (Elgharbawy, Schwarzhaupt, Frey, & Gauterin, 2017). To study the differences (in terms of vehicle interactions) between longitudinal and lateral directions, we present a skeleton of a multispring model with elliptic distribution, as shown in Figure 2 (Part II).

As shown in Figure 2 (Part II), A_1A_2 and B_1B_2 are the major and minor axes of the ellipse, respectively. Vehicle j is at the center of the ellipse. There is a spring between vehicle j and any point P on the ellipse. The spring between the ellipse and the vehicle j will compress under pressure when another road user enters it; which indicates the existence of risk between the two vehicles. Notably, all the springs in the elliptic curve have the same stiffness. We assume that when the other road user comes into the elliptic curve, it will compress the spring between itself and the vehicle producing the elliptical area. This results in the spring force, implying that there exists risk between them.

Acceleration and braking behaviors of a vehicle also have a significant impact on the vehicles around. A sudden emergency braking of a vehicle in front can cause a shock to the driver behind and can even create a rear-end collision.

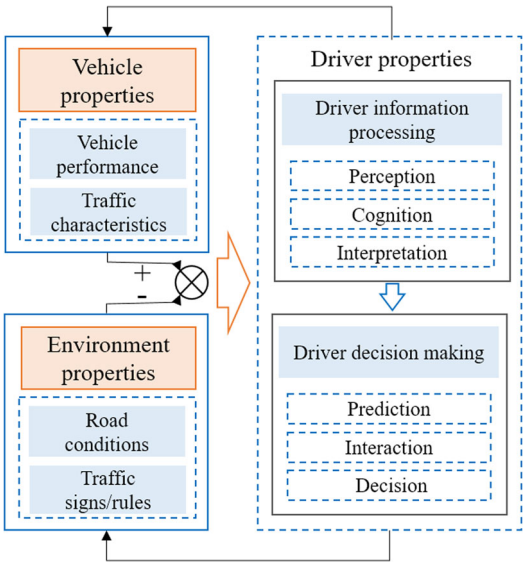

FIGURE 3 Flowchart of driver's behavior

Similarly, a vehicle with emergency acceleration can also cause road users ahead, particularly pedestrians, to dodge in fear. To determine the effects of these behaviors on driving risk while driving, we consider a spring oscillator model between the ellipse foci, as shown in Figure 2. We suppose that vehicle j is connected to each focus of the ellipse through another spring. Therefore, vehicle j remains at the center of the ellipse while traveling at a constant speed, approaches the left focus of the ellipse C_1 while the vehicle accelerates, and is close to the right focus of the ellipse C_2 while the vehicle decelerates.

To describe the interaction between different vehicles accurately, we introduce the concept of the elastic force of the spring and elastic energy stored. We present the modeling process of this combined model in detail in Section 3.

2.2 | Profiles of the behavioral decision-making module

In the traffic system, the driver is the receiver and processor of information, the controller of the "driver-vehicle-road" closed loop system, and also the part with the highest complexity. Moreover, the driver's behavior is directly sent to the traffic system, mainly determining the traffic operation state.

Moreover, as an agent, the driver will be affected depending on multiple sources of information from the environment. A survey conducted in the United States revealed that the driver receives more than 300 types of information and needs to make 75 decisions per km (Green, 2000; Chai, 2016). Hence, analyzing the driver's behavior is highly essential for behavioral decision making of intelligent vehicles.

Figure 3 shows that the driver's decision-making behavior can be affected by the surrounding objects and environments, such as lane lines, signs, guardrails, signal lights, and the visible greening of the surroundings. These can affect the driver's operation; hence, the driver's behavior needs to be analyzed from the perspective of the driver's psychology to drive an intelligent vehicle that imitates human drivers. Besides, we assume in Figure 3 that there is no need for obtaining information on the traffic environment and surrounding objects because it has been described in Figure 1.

Regarding the decision-making components, we design a model by considering multiobjectives to control the vehicle like a human driver. Intelligent vehicle decision making should aid autonomous driving by understanding human drivers' behaviors and strategies in real traffic environments. Most experienced human drivers have demonstrated the ability to dynamically choose the behavioral profiles that are safe, optimal in travel time, and ensure drivers' comfort. Thus, the behavioral decision-making process of intelligent vehicles needs to satisfy the requirement of drivers. The cost function is established to enable multigoals in the driving process. We employ the principle of least action to model the decision-making process based on the driver's driving target. The idea of the model and process of this module will be discussed in Section 4 in detail.

3 | METHODOLOGY OF VEHICLE INTERACTIONS MODELING

As mentioned earlier, this paper mainly focuses on risk assessment considering vehicle interactions. Therefore, in this section, we describe the methodology of vehicle interaction modeling; more specifically, we develop the proposed method based on driving risk analysis and a combined ellipse spring model (comprising a multispring model and a spring oscillator model), which can support the behavioral decision-making process.

3.1 | Driving risk analysis

System safety studies believe that hazard sources are the leading causes of accidents. According to Hammer's (1972, 2003) definition of risk, the hazard sources in the road transportation system include the kinetic and gravitational potential energy of vehicles and hazardous materials, such as fuel and other harmful chemicals and human errors, mechanical faults, poor road condition, and severe weather. Meanwhile, by considering that the decision-making algorithm of the intelligent vehicle depends on good environment perception and underlying control capability, we made the following four assumptions: (a) the vehicle and the road environments are in good conditions (additionally, the road is straight and without slope, and the gravitational potential energy of the vehicle is negligible); (b) drivers feel very safe if the time headway (THW) is more than 1.5 s in the longitudinal driving direction; (c) the

intelligent vehicle captures all the information in the surrounding road-traffic environments before making any decision; and (d) the intelligent vehicle has a favorable vehicle controller so that it can drive accurately depending on the reference trajectory, which is produced from the decision-making module.

One can conveniently calculate the kinetic energy based on the mass and velocity of the vehicle, and also determine the mass of vehicles by applying vision-based image-recognition technologies approximately or directly capture using vehicle-to-vehicle (V2V) devices. Similarly, the velocity can be obtained using sensor-based technologies, such as camera, radar, and V2V. However, it is quite challenging to determine the behavior of the drivers. The change of vehicle movement, particularly an unexpected change, significantly influences the safety of the transportation system. When a vehicle in front applies brake suddenly, a very short distance that is between vehicles is likely to cause a rear-end collision. Numerous researches have been conducted on this topic, and it has been agreed upon that the THW can be used for longitudinal risk assessment; additionally, the time for lane cross and lane change can be used for lateral risk control while driving. Therefore, the driver dynamically adjusts the distance between the surrounding road users and road boundaries depending on the driving speed while driving in the lateral and longitudinal direction. The behavioral adjustment is just like the numerous virtual springs with different lengths installed around the vehicle body. However, there will be a risk between the vehicle and the other road users when the spring is compressed, that is, when the stored elastic potential energy is higher than the acceptable level of that of the driver, who will take immediate actions to avoid more accumulation of elastic potential energy.

3.2 | The combined spring model

It is well known that the longitudinal driving risk relates to the THW; thus, we set 1.5 s as the threshold of THW according to the second assumption in Subsection 3.1. In the lateral direction, vehicles usually have the most significant influence on road users on the right and left adjacent lanes (Sun & Elefteriadou, 2012). Hence, as shown in Figure 2, the semimajor and semiminor axes are set as follows:

$$a = 1.5v_j \tag{1}$$

$$b = l_w \tag{2}$$

where a and b, respectively, denote the length of the semimajor and semiminor axes, that is, $a = jA_1 = jA_2 = 0.5A_1A_2$ and $b = jB_1 = jB_2 = 0.5B_1B_2$, v_j denotes the velocity of vehicle j, l_w denotes the lane width; besides, we set $l_w =$ 3.5m. In addition, a and b are subject to the condition $a \geq b$.

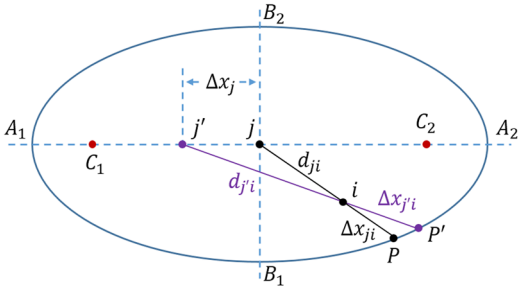

FIGURE 4 The calculation principle of the combined spring model

Therefore, the spring will compress and store the elastic potential energy when another vehicle i enters the ellipse. Hence, it follows that:

$$F_{ji} = k_1 \Delta x_{ji} \tag{3}$$

$$U_{ji} = \int_0^{\Delta x_{ji}} k_1 d\Delta x_{ji} \tag{4}$$

where F_{ji} denotes the elastic force between vehicles j and i, k_1 is the spring stiffness in the ellipse, Δx_{ji} is the spring compression length, and U_{ji} is the elastic potential energy. Additionally, F_{ji} and U_{ji} denote the driving risk between vehicles j and i, respectively.

Figure 4 illustrates the calculation principle of the combined spring model. It shows that the points j and i represent vehicles j and i, respectively. The length of the compressed spring is denoted by Δx_{ji} if vehicle j drives at a steady speed, and it is denoted by $\Delta x_{j'i}$ if vehicle j is accelerating, and vice versa during braking.

As shown in Figure 4, when vehicle j is driving at a constant speed, the equivalent forces depend on the relationships among the various movements of road users according to the proposed method (Zheng et al., 2018). The interaction between vehicle j and a vehicle at A_2 is given by:

$$F_{j,A_2} = \frac{m_j v_j^2}{2a} \tag{5}$$

In this study, we calculate the spring stiffness k_1 in the ellipse as follows:

$$k_1 \Delta x_{ji} = \frac{1}{2} m_j v_j^2 \left(\frac{1}{d_{ji}} - \frac{1}{a} \right) \tag{6}$$

where d_{ji} denotes the distance between vehicles i and j. In addition, Δx_{ji} is expressed as follows:

$$\Delta x_{ji} = a - d_{ji} \tag{7}$$

Therefore,

$$k_1 = \frac{m_j v_j^2}{2a d_{ji}} \tag{8}$$

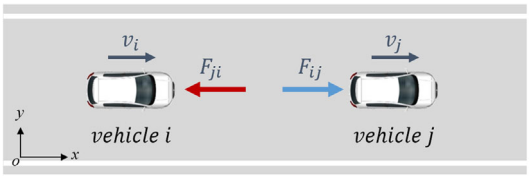

FIGURE 5 A specific car-following scenario

From Equation (8), one observes that the stiffness of the spring dynamically varies with the speed of vehicle j and the relative distance between vehicles j and i. This implies that the higher the mass and speed, the higher the risk; whereas the smaller the relative distance, the higher the risk.

When vehicle j is driving with a constant acceleration or deceleration, the vehicle will be subject to an inertial force given by:

$$F_{\text{inertia},j} = m_j a_j = 2k_2 \Delta x_j \tag{9}$$

where $F_{\text{inertia},j}$ denotes the inertial force on the vehicle j, m_j denotes the mass of the vehicle j, a_j denotes the acceleration of the vehicle j, the stiffness of the spring is denoted by k_2, and Δx_j denotes the length of the compressed spring.

Notably, the spring forces are similar to what several authors refer to as social force (Helbing & Tilch, 1998; Lin, Ma, Li, & Wang, 2016). The stiffness of the multispring k_1 and the spring oscillator k_2 represents the different motivations of the driver, which an individual experiences in each vehicle. As these spring forces do not satisfy Newton's laws, such as *actio = reactio* (Helbing & Tilch, 1998), herein, we assume that in a specific car-following scenario (as shown in Figure 5), the physical property (i.e., the same vehicle type and mass, $m_i = m_j$), the state of motion (i.e., $v_i = v_j =$ const), and the driver of the front and the following vehicles are same. Hence, the spring force between vehicle i and j satisfies $F_{ij} = -F_{ji}$. That is, the model satisfies Newton's third law in this specific case. Therefore, inertial forces of the front vehicle (vehicle j) $F_{\text{inertia},j}$ and the spring forces F_{ij} and F_{ji} relate as follows:

$$F_{\text{inertia},j} = F_{ij} - F_{ji} \tag{10}$$

From Equations (3), (8), (9), and (10), the stiffness of the spring between the ellipse foci is calculated as follows:

$$k_2 = \frac{1}{2}k_1 = \frac{m_j v_j^2}{4ad_{ji}} \tag{11}$$

As Figure 4 illustrates, we set the positions of vehicles i and j to be (x_i, y_i) and $(0, 0)$, respectively. Then, the compressed spring length, Δx_{ji}, is calculated as follows:

$$\Delta x_{ji} = \frac{d_{ji}ab}{\sqrt{b^2 x_i^2 + a^2 y_i^2}} - d_{ji} \tag{12}$$

Therefore, by applying Equations (8) and (12), the elastic force and its direction on vehicle i based on constant speed driving conditions is obtained by:

$$F_{ji} = \frac{bm_j v_j^2}{2\sqrt{b^2 x_i^2 + a^2 y_i^2}} - \frac{m_j v_j^2}{2a} \tag{13}$$

$$\theta = \arctan\frac{y_i}{x_i} \tag{14}$$

where θ denotes the angle between the velocity of vehicle j and the line connecting the two vehicles.

As shown in Figure 4, the straight line $j'p'$ can be expressed as:

$$y = \frac{y_i}{x_i + \Delta x_j}x + \frac{y_i \Delta x_j}{x_i + \Delta x_j} \tag{15}$$

The point p' is the intersection of the line $j'p'$ and the ellipse. Hence, the coordinates of p' can be calculated as follows:

$$x_{p'} = \frac{1}{W_1 + W_2} \times \left[-W_2 \Delta x_j + \sqrt{W_2^2 \Delta x_j^2 + (W_1 + W_2)(W_1 a^2 - W_2 \Delta x_j^2)}\right] \tag{16}$$

$$y_{p'} = \frac{y_i}{x_i + \Delta x_j}\left(x_{p'} + \Delta x_j\right) \tag{17}$$

where

$$W_1 = b^2\left(x_i + \Delta x_j\right)^2 \tag{18}$$

$$W_2 = a^2 y_i^2 \tag{19}$$

Therefore, the compressed spring length, $\Delta x_{j'i}$, given as:

$$\Delta x_{j'i} = \left(\frac{W_3 - W_2 \Delta x_j}{W_1 + W_2} - x_i\right)\sqrt{1 + \left(\frac{y_i}{x_i + \Delta x_j}\right)^2} \tag{20}$$

where

$$W_3 = \sqrt{W_2^2 \Delta x_j^2 + \left(W_1 + W_2\right)\left(W_1 a^2 - W_2 \Delta x_j^2\right)} \tag{21}$$

Similarly, the elastic force and its direction on vehicle i based on acceleration driving conditions is obtained as:

$$F_{ji} = \frac{m_j v_j^2}{2ad_{ji}} \Delta x_{j'i} \tag{22}$$

$$\theta = \arctan \frac{y_i - y_j}{x_i + \Delta x_j - x_j} \tag{23}$$

Hence, in this study, we have applied the elastic force of the spring and its stored elastic potential energy to describe the interaction between vehicles.

4 | BEHAVIORAL DECISION-MAKING MODEL

Intelligent vehicles can evaluate driving risk in a dynamic traffic environment by using the elastic force of the spring and its stored elastic potential energy based on the vehicle interaction model. Besides, it is more desirable if they could drive vehicles in the same way as human drivers. Hence, in this section, we present a behavioral decision-making module to explain the process of incorporating and applying the principle of least action and establishing a multiobjective decision-making model. More specifically, first, we choose the main driving goals in the process of driving, then establish the cost function for the behavioral decision-making model based on the principle of least action regarding the driver's driving target. Finally, we establish a mathematical model of multiobjective decision making to describe the decision process.

4.1 | Drivers' various driving goals

Drivers have different specific driving goals while driving, such as no collisions, avoiding violation of traffic rules, reaching the destination as soon as possible, achieving mobility, safety and comfort, and low fuel consumption.

However, some drivers have specific requirements to ensure comfort and minimal fuel consumption in their driving processes. For example, if the driver or any of the passengers are susceptible to motion sickness, they will need more comfort; in that case, the driver will drive carefully to avoid excessive acceleration and deceleration. Moreover, people who engage in energy-conserving practices, including some commercial vehicle drivers, may turn the engine off while running on a long downhill section, or while waiting at an intersection to reduce fuel consumption. The requirement for high comfort or low fuel consumption is not universal for all drivers. However, safety and efficiency are the peculiar targets of all drivers in all their driving processes.

Therefore, "safety" and "high efficiency" are chosen as the main objectives that are pursued by drivers in all their driving processes. Herein, safety includes no collision and safe driving, while high efficiency includes avoiding the violation of traffic rules and getting to the destination as soon as possible. In subsequent subsections, we will determine them from an overall perspective and obtain the extreme values while driving depending on the multiobjective decision-making model, which is based on the principle of least action.

4.2 | The principle of least action while driving

In physics, the principle of least action is applied to demonstrate extreme-value processes. The principle of least action is not only a fundamental principle of conservation and symmetry, which is very crucial in physics, but it is also the most general principle (Coopersmith, 2017; Landau & Lifshitz, 2013). If we use S to denote the action, this principle can be expressed as $\delta S = 0$. All the universal laws of physics so far can be expressed by the principle of least action (Coopersmith, 2017; Landau & Lifshitz, 2013).

According to the principle of least action, whenever there is more than one way to implement a process, it is of paramount importance to choose the method that minimizes the product of time and energy (Coopersmith, 2017). Following the earlier mentioned main objectives, each driver has a goal of maximizing profit and minimizing loss: the "profit" represents safety and mobility, while the "loss" represents collisions and violations. Otherwise, the kinetic energy of the vehicle and the interactions between the vehicle and its surrounding traffic environment are used to determine the safety of the driving processes, while the travel time is used to determine the efficiency of the driving processes. If the least action is used to represent the maximum safety and efficiency value during the driving process, then we have that:

$$S = \int_{t_0}^{t_f} L\, dt = \int_{t_0}^{t_f} (T - U)\, dt \tag{24}$$

where L ($T - U$ for the cases considered) is called the Lagrangian, T and U denote the kinetic and potential energies of the vehicle, respectively. Additionally, the kinetic energy T denotes the risk from the energy of the vehicle, and an accident is an abnormal transfer of energy in accordance with the energy transfer theory (Fu, 2013). The process by which a vehicle accelerates from rest to a certain speed is actually a way of increasing its energy storage. The stored energy will be released and transferred if a collision occurs at any point, and this will lead to elastic and plastic deformation. Consequently, the kinetic energy, T, increases as the potential risk increases. The potential energy U denotes the relationship between the vehicle and the surrounding traffic environment. The greater the $-U$, the greater the risk of the surrounding traffic environment to the vehicle. Notably, the potential energy herein is not the gravitational potential energy in the traditional sense. It can be understood because a state changes owing to the interaction between vehicle and environment. For example, if an adjacent vehicle approaches the subject vehicle from a distance and passes the subject vehicle, the potential energy increases and then decreases during this process, in

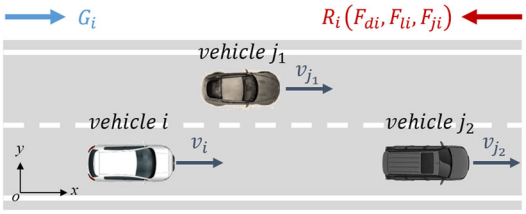

FIGURE 6 Typical driving scenario

accordance with the vehicle interaction model in Section 2. Furthermore, t_0 and t_f denote the initial time and the final time, respectively. Additionally, herein, the integral over time has two meanings. First, it represents the accumulation of risks in the driving processes; second, it represents the traffic efficiency of driving a certain length of the road. Therefore, the smaller the value of S, the safer and more efficient the driving processes will be.

4.3 | Mathematical model of multiobjective decision making

The driving process is visually described as a process in which the vehicle is being pulled by gravity in the horizontal direction, as shown in Figure 6. Therefore, it is assumed that there is an attractive force in the driving direction. Additionally, the acceleration due to the pseudo-gravity, g_h, is associated with the driver's expected velocity or mobility. The attractive force is expressed as:

$$G_i = m_i g_h \tag{25}$$

where m_i denotes the mass of vehicle i and g_h denotes the acceleration due to the pseudo-gravity. We define g_h by:

$$g_h = k\frac{v_{\text{der}}}{v_{\text{limit}}}g \tag{26}$$

where k denotes a constant (herein, we take $k = 0.2$), v_{der} denotes the driver's expected speed, v_{limit} denotes the speed limit, and g denotes the gravitational acceleration.

Furthermore, drivers always avoid violations depending on the traffic laws, such as obeying the speed limit, v_{limit}, while driving; therefore, we use a constraint resistance force, F_{di}, to denote the influence of traffic rules on drivers. We define the constraint resistance force, F_{di}, due to traffic rules as:

$$F_{di} = m_i g_h \left(\frac{v_i}{v_{\text{limit}}}\right)^{\tau} \tag{27}$$

where τ denotes a calibration parameter (herein, we take $\tau = 1$).

The lane lines or lane boundaries usually have a significant impact on the driver. In our previous study (J. Wang, Wu, & Li, 2015), this impact is described by applying a lane marker force defined as follows:

$$F_{li} = 1.5 m_i l_t \left(\frac{l_w}{2} - r_{li}\right)^{k_2} \tag{28}$$

where l_t denotes the lane marker type (herein, we take $l_t = 3$ for the dotted line and $l_t = 2$ for the solid line), r_{li} denotes the distance between vehicle i and the lane marker, and k_2 is a constant (we take $k_2 = 1.2$).

The increasing number of vehicles has turned the traffic environments into an extremely complicated system. This analysis can be simplified by studying a typical driving vehicle. Figure 6 shows the Lagrangian for a vehicle in the naturalistic driving scenario, which can be obtained using the following equation:

$$L = \frac{1}{2}m_i v_i^2 - \int_{t_0}^{t_f} \left(R_i - G_i\right) v_i dt \tag{29}$$

where m_i denotes the mass of the vehicle i, G_i denotes the attractive force acting on the vehicle, and R_i denotes the multiresistance force, which includes the constraint resistance force F_{di}, the lane marker force F_{li}, and the elastic force F_{ji}.

Therefore, the action of the vehicle while driving can be obtained by:

$$S = \int_{t_0}^{t_f} \left[\frac{1}{2}m_i v_i^2 - \int_{t_0}^{t_f} \left(R_i - G_i\right) v_i dt\right] dt \tag{30}$$

Additionally, S is also the cost function of the multiobjective decision-making model. The cost function considers safety and high efficiency to optimize the driving decision-making process. Furthermore, we will use particular instances to illustrate this cost function in the next section.

5 | ANALYSIS OF PARTICULAR CASES AND SIMULATION EXPERIMENTS

In this section, we conduct some simulation experiments to confirm the value of S and validate the effectiveness of the proposed model in particular scenarios.

As mentioned earlier in the Introduction section, Waymo vehicles usually have difficulties in making a decision to turn left at an unprotected T-intersection in traffic. Therefore, herein, we designed an unprotected T-intersection for particular scenarios to validate the effectiveness of the proposed method of the behavioral decision-making model, as shown in Figure 7. As Figure 7 shows, the white vehicle (vehicle i) denotes the subject vehicle, while the brown one (vehicle j) denotes the lead vehicle in traffic flow. We simplified the traffic flow for this single vehicle j to facilitate the

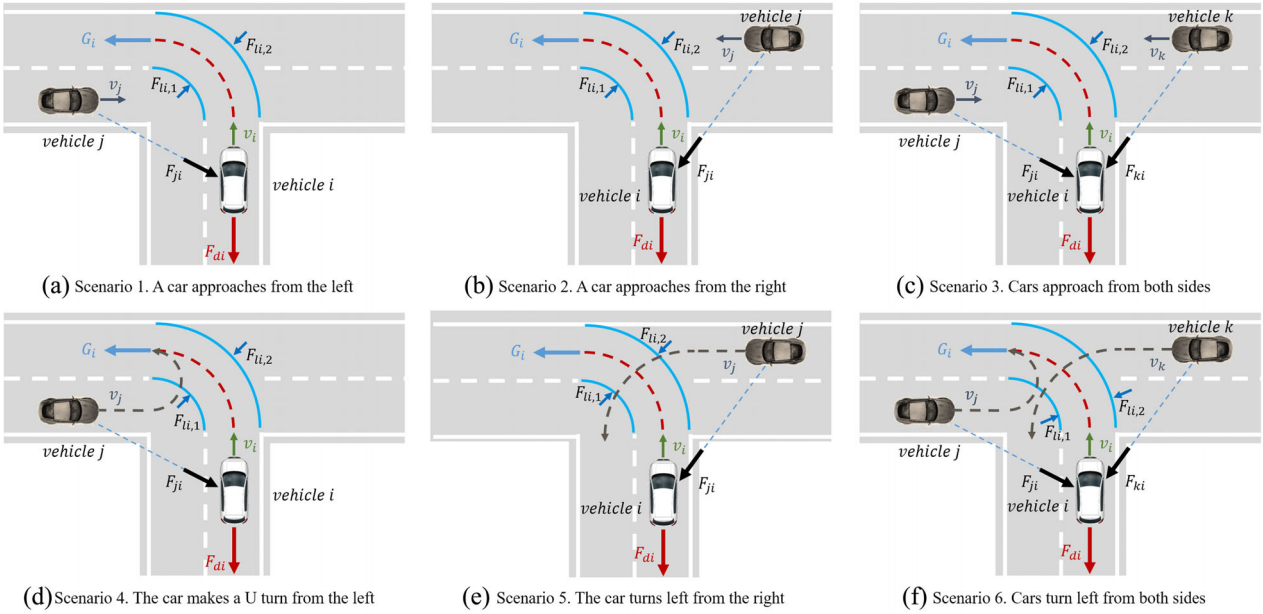

(a) Scenario 1. A car approaches from the left (b) Scenario 2. A car approaches from the right (c) Scenario 3. Cars approach from both sides

(d) Scenario 4. The car makes a U turn from the left (e) Scenario 5. The car turns left from the right (f) Scenario 6. Cars turn left from both sides

FIGURE 7 Conflict scenarios of left-turn at an unprotected T-intersection

analysis. When the subject vehicle, i, wants to turn left at the T-intersection, it can encounter any of these six situations: (a) a vehicle approaches the T-intersection from the left; (b) a vehicle approaches the T-intersection from the right; (c) vehicles approach the T-intersection from both sides; (d) a vehicle makes a U-turn at the T-intersection from the left side; (e) a vehicle turns left at the T-intersection from the right side; and (f) vehicles turn left at the T-intersection from both sides. The task of the subject vehicle, i, is to drive from the red reference path to the other side without crossing the blue boundary and without colliding with other road users.

5.1 | Decision-making model based on particular scenarios

It is known that the subject vehicle is subject to four types of forces: the attractive force G_i, the constraint resistance force F_{di}, the lane marker force F_{li}, and the elastic force F_{ji}. Figure 7 illustrates these forces. The research conducted in this study is based on the coordinate system of the subject vehicle. Hence, the cost function of the multiobjective decision-making model can be obtained by:

$$S = \int_{t_0}^{t_f} \left[\frac{1}{2} m_i v_i^2 - \int_{t_0}^{t_f} \left(F_{di} + F_{ji} + F_{ki} - G_i + F_{li,1} - F_{li,2} \right) v_i dt \right] dt \tag{31}$$

Maupertuis' principle of least action states that along with a real trajectory, an action is stationary based on the virtual variation of the trajectory (Coopersmith, 2017; Landau & Lifshitz, 2013). The actual action in the driving process may be time-varying due to the subjective factors of the driver. However, in theory, there is a path for which action never changes. Herein, this path corresponds to the safest and most efficient driving process. According to the principle of least action, the variation of the action is equal to zero during this process. Thus, we have that:

$$\delta S = \int_{t_0}^{t_f} \delta L \, dt = 0 \tag{32}$$

The Lagrangian can be decomposed into Cartesian coordinates to facilitate the analysis. So, we get that:

$$L_X = \frac{1}{2} m_i v_{ix}^2 - \int_{t_0}^{t_f} \left(F_{di} + F_{ji} \cos\theta_{ji} + F_{ki} \cos\theta_{ki} - G_i \right) v_{ix} dt \tag{33}$$

$$L_Y = \frac{1}{2} m_i v_{iy}^2 - \int_{t_0}^{t_f} \left(F_{ji} \sin\theta_{ji} + F_{ki} \sin\theta_{ki} + F_{li,1} - F_{li,2} \right) v_{iy} dt \tag{34}$$

where θ_{ji} denotes the angle between the elastic force F_{ji} and the constraint resistance force F_{di}, while θ_{ki} denotes the angle between the elastic force F_{ki} and the constraint resistance force F_{di}. We remark that the counterclockwise direction is positive.

By substituting Equations (33) and (34) into the Euler–Lagrange equation, we obtain the following equations:

$$m_i \dot{v}_{ix} - \left(F_{di} + F_{ji}\cos\theta_{ji} + F_{ki}\cos\theta_{ki} - G_i\right) = 0 \quad (35)$$

$$m_i \dot{v}_{iy} - \left(F_{ji}\sin\theta_{ji} + F_{ki}\sin\theta_{ki} + F_{li,1} - F_{li,2}\right) = 0 \quad (36)$$

Equations (35) and (36) satisfy Newton's second law of motion. Therefore, if the mechanical balance is always satisfied during the driving process in both the longitudinal and lateral directions, then the process with the least action is the safest and most efficient optimal process.

However, the mechanical balance is the only necessary condition of this proposed method of the behavioral decision-making model, and the cost function, S, is the key factor that will determine whether the vehicle is moving or not. Thus, the cost function, S, given by Equation (31), can be calculated using the action along the reference path. In addition, Equations (35) and (36) are used for calculating both the least action S^* in each situation and the longitudinal and lateral control of the subject vehicle. If all of our assumptions are valid, this approach will make the intelligent vehicle behave in the same way as human drivers.

5.2 | Simulation results

In this study, the driving scenarios are generated by a MATLAB application: driving scenario designer. The ego-vehicle is equipped with radars and a front camera to detect its surrounding objects. Position data and vehicle dynamics of all vehicles are recorded for algorithm verification.

Table 1 shows the algorithm of the behavioral decision-making model. The subject vehicle, i, detects the initial positions and velocities of the other surrounding vehicles, such as vehicles j and k. Then, we load the least action S^* from the matrix containing the least actions of optimal paths in all possible situations. Finally, the algorithm gives the output instructions when the vehicle crosses the T-intersection or waits for another chance through the vehicle controller by comparing the values of S and S^*.

During the simulation experiments, we first assume that the other vehicles except for the subject vehicle, i, are driving at a constant speed. The simulation experiments are performed 100 times based on the conditions of the travel speed of 7–25 m/s and initial vehicle distance of 15–60 m for the six scenarios. Based on each condition of the corresponding speed and the initial distance of the other vehicles in these three scenarios, simulation experiments are used to calculate the value of the cost function, S, as shown in Figures 8a–c and 9a–c, which we called cost function maps. Moreover, we also considered whether the subject vehicle, i, chooses to pass the T-intersection in each simulation process, as shown in Figures 8d–f and 9d–f, which we called pass-waiting judgment charts. The green circle in the pass-waiting judgment charts indicates that the vehicle chooses to cross the T-intersection, whereas the red star indicates the opposite. Additionally, each green circle is related to a corresponding bar in the cost function map, while the red dots correspond to valleys. Hence, we can easily identify whether the target vehicle is passing or not, and also obtain the value of the corresponding cost function.

First, we analyze the simulation results in scenarios 1–3. As shown in the pass-waiting judgment charts (Figure 8d–f), the subject vehicle, i, did not choose to pass the T-intersection when the time to intersection (TTI) is less than 2 s in most situations and the distance between the subject vehicle, i, and the other vehicles on both sides should be at least 20 m in these three scenarios. Notably, the TTI needs to be greater than 2.25 s to be safe in scenarios 2 and 3.

Simultaneously, we observed a surprising phenomenon that when the speed of another vehicle is high and the relative distance is small, for example, TTI is less than 0.9 s in scenarios 1 and 3, or TTI is less than 1.32 s in scenario 2, that is, the TTI is very small; the subject vehicle, i, unexpectedly chose to pass the T-intersection. It must be dangerous and impassable for a TTI-based decision-making algorithm in these three situations. However, the subject vehicle, i, which depends on the method of the behavioral decision-making model proposed in this study, chooses to pass the T-intersection based on these three situations. This unusual phenomenon draws our attention to the simulation data. We surprisingly observed that the subject vehicle, i, would move forward slowly at the beginning of these situations and pass through the T-intersection as soon as vehicle, j, drives out of the intersection in scenario 1. This is similar to scenarios 2 and 3. This behavior is similar to that of some aggressive drivers.

Let us analyze the bar on the left-hand side of the cost function map. As the three cost function maps show, when the velocities of the vehicles j and k are constant; the smaller the initial distance, the greater the value of the cost function, S. Similarly, when the initial distance is constant; the higher the speed, the greater the value of the cost function, S. Further, as the value of the cost function, S, increases, the decision-making algorithm observes that an accident will occur if the subject vehicle, i, passes at this moment, so the behavioral decision-making model chooses not to pass the T-intersection.

The other vehicles are driving straight in the first three scenarios. Herein, we turn to the last three scenarios in Figure 7 in which other vehicles make left turns at the T-intersection. As shown in the pass-waiting judgment charts (Figure 9d–f), the simulation results of the following three scenarios are quite different from the first three scenarios. In scenario 4, the subject vehicle, i, chooses to wait in two-thirds of the situations, when TTI is less than 2.3 s. However, vehicle i chooses, and it decides to cross the T-intersection in the other one-third of the situations. Moreover, most of the above one-third of the cases

TABLE 1 Algorithm: Behavioral decision making

Input	$t_{nd}, t, F_{ji}, G_i, F_{di}, F_{li}, x_i(1:t_{nd}), y_i(1:t_{nd}), r_{li}(1:t_{nd}), \theta_{ki}(1:t_{nd}), \theta_{li}(1:t_{nd}), \theta_{ji}(1:t_{nd}) Yaw(1:t_{nd}), d_{ji}, m_i, m_j, g, v_{\text{der}}, v_{\text{limit}}, k, k_2, \tau, l_t, l_w$
Output	S
1	Initialize $t \leftarrow 1, k \leftarrow 0.2, k_2 \leftarrow 1.2, \tau \leftarrow 1,\ l_t \leftarrow 3,\ l_w \leftarrow 3.5, S(int) \leftarrow 0,\ T(int) \leftarrow 0, U(int) \leftarrow 0$
2	Get the initial position of surrounding vehicles (x_j, y_j)
3	Get the initial velocity of surrounding vehicles (v_{xj}, v_{xj})
4	Load S^* from map
5	Define the attractive force: $G_i = m_i k \frac{v_{\text{der}}}{v_{\text{limit}}} g$
6	Define the constraint resistance force: $F_{di} = G_i(\frac{v_i}{v_{\text{limit}}})^{\tau}$
7	Define the lane marker force: $F_{li} = 1.5 m_i l_t [\frac{l_w}{2} - r_{li}(t)]^{k_2}$
8	Define the kinetic energy of the vehicle: $T = \frac{1}{2} m_i v_i^2$
9	**while** $t \le t_{nd}$ (t_{nd} denotes the final time of simulation) **do**
10	$x_j \leftarrow x_j + (t-1)\, v_{xj}$
11	$y_j \leftarrow y_j + (t-1)\, v_{yj}$
12	**for** $j = 1$ to n (n denotes the number of surrounding vehicles) **do**
13	Calculate the spring stiffness: $k_{j,2} = \frac{m_j v_j^2}{2 d_{ji}}$
14	Calculate the distance between vehicles i and j: $d_{ji} = \sqrt{(x_j - x_i)^2 + (y_j - y_i)^2}$
15	Calculate the spring compressed length: $\Delta x_{ji} = \frac{\sqrt{a^2 (x_j - x_i)^2 + b^2 (y_j - y_i)^2}}{d_{ji}} - d_{ji}$
16	**if** $\Delta x_{ji} > 0$
17	Calculate the elastic force between vehicles j and i: $F_{ji} = k_j \Delta x_{ji}$
18	Calculate the angle between the velocity of vehicle j and the line connecting the two vehicles: $\theta_{ji} = \arctan \frac{y_j - y_i}{x_j - x_i} - Yaw(t)$
19	**else**
20	$F_{ji} = 0$
21	**end if**
22	**end for**
23	Calculate the potential energy of the vehicle: $U = (-G_i + F_{di} + \sum F_{ki} \cos\theta_{ki} + \sum F_{ji} \cos\theta_{ji})[x_i(t) - x_i(t-1)] + (\sum F_{ji} \sin\theta_{ji} + \sum F_{ki} \sin\theta_{ki} + \sum F_{li})[y_i(t) - y_i(t-1)]$
24	Calculate the cost function of the multiobjective decision-making model: $S = S + T - U$
25	**end while**
26	**if** $S > S^*$ **then**
27	Output ("waiting," the vehicle i is waiting for another chance)
28	**else**
29	Output ("pass," the vehicle i is passing the T-intersection)
30	**end if**

have low TTI values, that is, less than 1.35 s. In scenario 5, the subject vehicle passes the T-intersection successfully in most of the instances, and the TTI value of the vast majority of the waiting scenarios is between 0.87 and 1.6 s. All the situations that have TTI values less than 2.25 s are waiting cases in scenario 6.

The cost function maps of scenarios 4–6 are shown in Figure 9a–c. Similarly, the changing trend of the value of the cost function, S, is generally consistent with the first three scenarios. The results show that the cost function can be used not only in situations where the other vehicles are going straight, but also in cases where they are turning. The greater the value of the cost function, S, the higher the risk degree of the traffic scenario. However, there are few abnormal values in scenario 2 as shown on the right-hand side of Figure 9b. The four bars in the figure are quite shorter than the adjacent bars. To confirm this situation, we rechecked the simulation video and data and found that is because the side of the vehicle, k, is facing the subject vehicle, i, in these scenarios. According to the combined spring model, the side

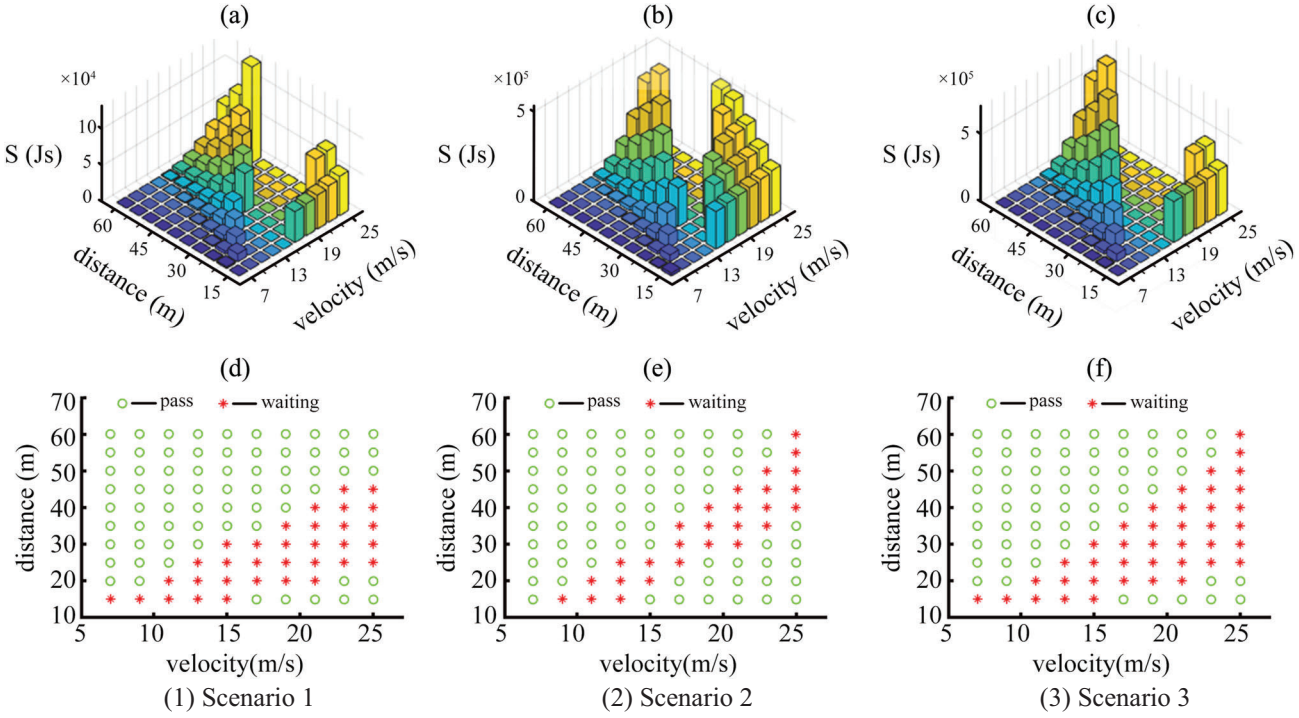

FIGURE 8 Simulation results (scenarios 1–3)

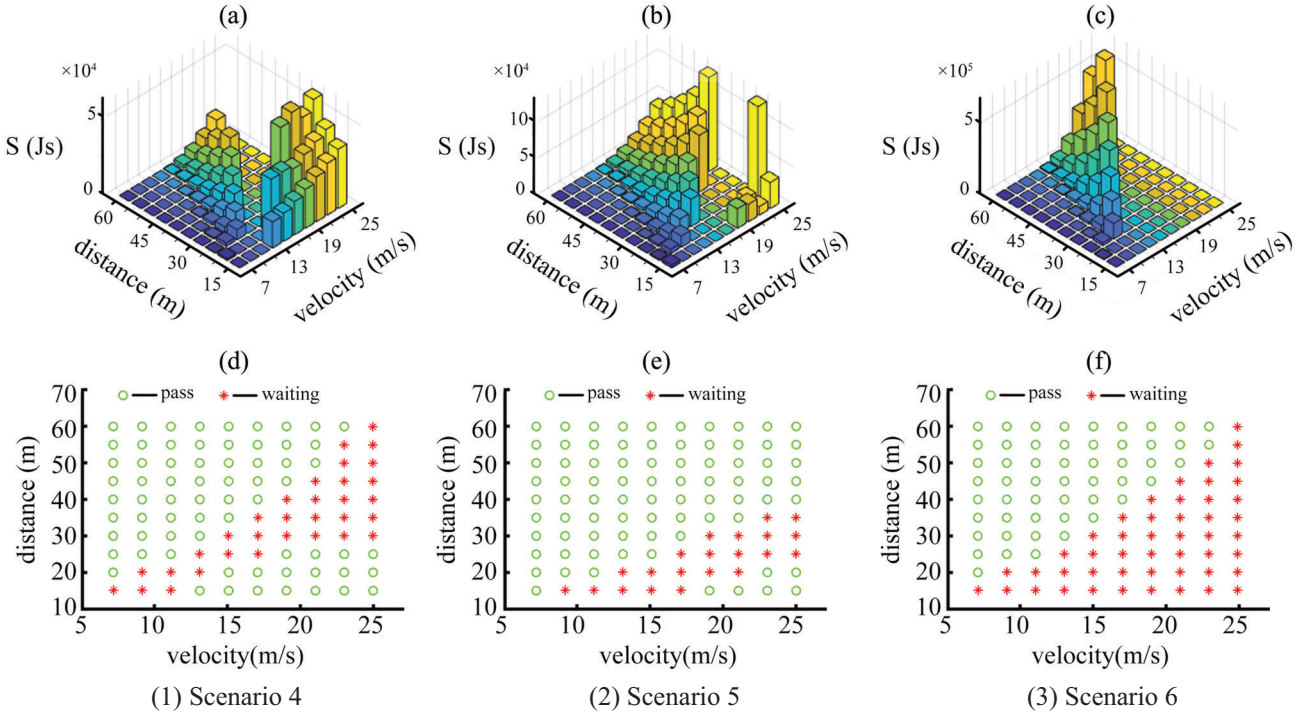

FIGURE 9 Simulation results (scenarios 4–6)

of the car has the minimum elasticity; hence, the phenomenon occurs.

In addition, the value of the cost function, S, is time-varying with the speed and relative distance of the other vehicle based on the cost function map. Therefore, when the subject vehicle, i, detects the deceleration of the vehicle j, the value of the cost function, S, decreases. One can observe that vehicle j intends to let go in this situation, and the proposed behavioral decision-making algorithm can decide to drive across the T-intersection when the value

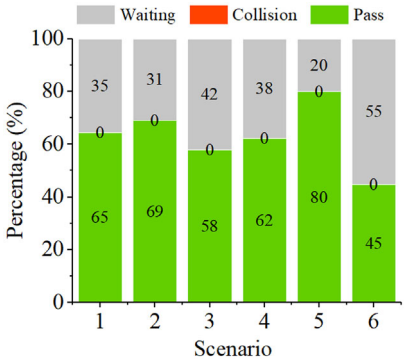

FIGURE 10 Simulation results of behavioral decision-making model

of the cost function, S, decreases to an appropriate level. Because sensors can accurately monitor the motion of the object vehicle, this decision-making model is even better than a human driver at recognizing the intentions of the other vehicles.

The cost function map is also called the decision-making map of a vehicle when it turns left at the T-intersection. This can be used to guide the decision-making control of intelligent vehicles in this scenario. In addition, this method can also be applied to other driving scenarios.

5.3 | Comparative analysis with TTI threshold method

Figure 10 shows the statistics of the subject vehicle choosing to wait or pass in the six scenarios. Each scenario was simulated 100 times. As shown in Figure 10, the gray bar indicates that vehicle i chooses to wait; the green bar indicates that the subject vehicle chooses to pass the T-intersection and successfully passes; and the orange bar indicates that the subject vehicle chooses to pass the T-intersection but makes a collision. However, the subject vehicle does not cause an accident according to our behavioral decision-making algorithm. The pass rate from scenarios 1 to 6 is 65%, 69%, 58%, 62%, 80%, and 45%, respectively. The results show that the impact of the left car (vehicle j) on the subject vehicle is greater than that of the right car (vehicle k) because the pass rates in scenarios 1 and 4 are less than those in scenarios 2 and 5, respectively. However, the pass rate in the scenario, which contains two other vehicles (scenarios 3 and 6), is lower than that in other single-vehicle scenarios (scenarios 1, 2, 4, and 5). This suggests that scenarios 3 and 6 are more dangerous than scenarios 1, 2, 4, and 5. Similarly, it was found that the subject vehicle will be more cautious in left-turn scenarios (scenarios 4–6) than in the straight-driving scenarios (scenarios 1–3).

To verify the effectiveness of the proposed behavioral decision-making algorithm, we utilized the TTI threshold to conduct total 5,400 simulations in six scenarios under the same simulation conditions. Figure 11 shows the simulation results. We set the simulation situation based on different TTI threshold from 1 to 9 s. As shown in Figure 11, each situation was simulated 100 times. The pass rate reaches an extremely high value if the TTI threshold is less than 2 s in all the six scenarios. The maximum pass rates

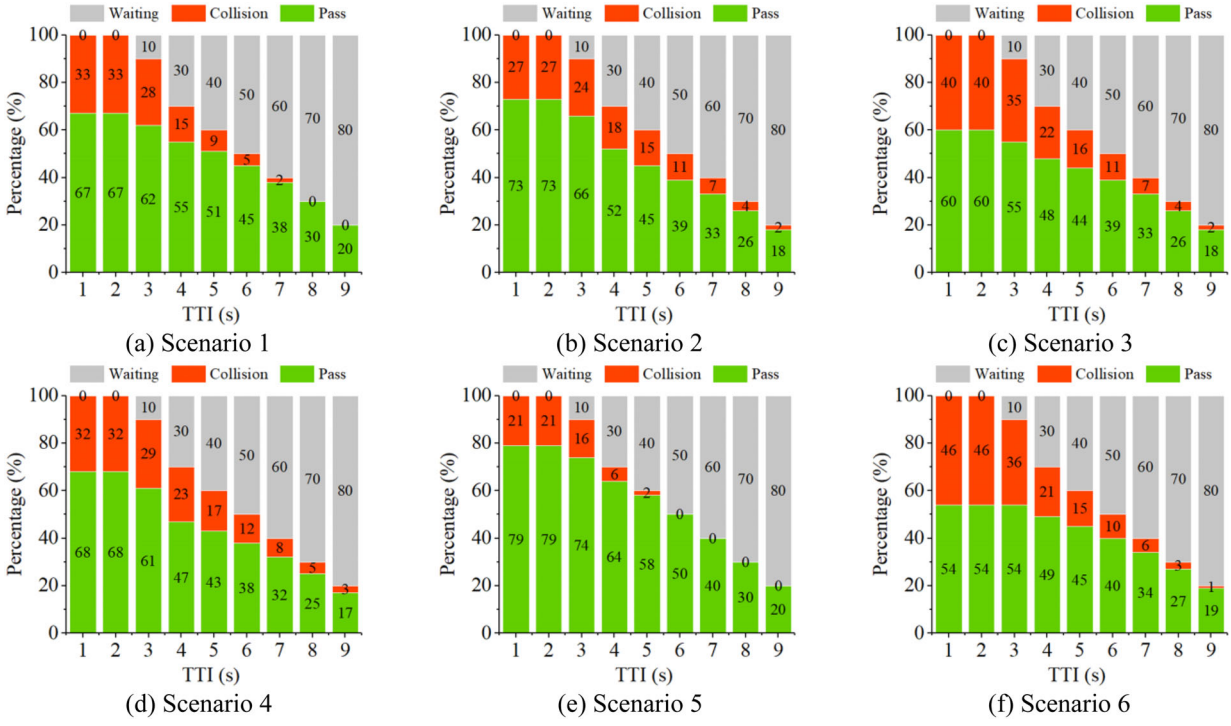

FIGURE 11 Simulation results of TTI thresholds

from scenarios 1 to 6 are 67%, 73%, 60%, 68%, 79%, and 54%, respectively. However, higher pass rates are accompanied by higher collision rates, that is, the smaller the TTI threshold, the more successful will be the pass cases as well as collisions. Hence, TTI thresholds need to be raised to improve driving safety. As TTI increases, the collision rate decreases, whereas the number of waiting cases increases and the traffic efficiency decreases.

Similarly, the simulation results based on the TTI threshold show the same change trend of the pass rate with the behavioral decision-making model. As shown in Figure 11, with the same TTI threshold, the pass rates of scenarios 2 and 5 are higher than those of scenarios 1 and 4 in most cases, respectively. The scenario, which contains two vehicles (scenarios 3 and 6), indicates more dangerous situation than in other single-vehicle scenarios (scenarios 1, 2, 4, and 5) because usually the collision rates in the former are much higher than those in the latter.

A comparison of the behavioral decision-making model with the TTI threshold method reveals that the former can always avoid collision accidents on the premise of ensuring certain efficiency, and it can achieve 97.01%, 94.52%, 96.67%, 91.18%, 101.27%, and 83.33% of TTI's maximum pass rate in scenarios 1–6, respectively. Indeed, if multiple TTI threshold combinations are used, the collision rate can be reduced. Therefore, multiple thresholds will be adjusted for different scenarios. However, this will severely impact the establishment of the decision-making model. Thus, the behavioral decision-making model has more advantages in ensuring traffic safety and improving traffic efficiency than the TTI-based threshold method.

6 | APPLICATIONS AT STANDARD INTERSECTIONS

Previous sections discuss conflict scenarios of left-turn in an unprotected T-intersection. In this section, we try to apply the behavioral decision-making algorithm to standard intersections.

At a standard two-lane intersection, the subject vehicle usually has four types of possible movements, that is, straight-driving, left-turn, right-turn, and turn-around, shown as the red dotted lines in Figure 12. The red points represent conflicts between the subject vehicle and other vehicles, and there are totally 28 conflict situations. Generally, the straight-driving situations are all protected scenarios at a standard multilane intersection, so we do not analyze these situations. Denote by X^iY^j the path from X^i to Y^j. When the subject vehicle turns right, there exists a possible conflict between A^2a^1 and D^2b^1, which is similar to scenario 2 at a T-intersection. When the subject vehicle turns around, there are three possible conflict situations, namely, A^1a^2 to D^2b^1, A^1a^2 to B^1a^2, and A^1a^2 to C^1a^2, which are similar to scenarios 1, 4, and 2 at T-intersections, respectively. Finally, there are eight conflicts between the subject vehicle and other vehicles during left-turning. Compared with an unprotected T-intersection, if we do not take into account the conflict situations of other vehicles, there are three extra complicated conflict scenarios at the intersection, namely, A^1d^2 to D^1d^2 and C^1a^2, A^1d^2 to D^1c^2 and B^1a^2, and A^1d^2 to B^1a^2 and C^2a^1. Herein, we name the above three conflicts as scenarios 7–9, respectively. This section analyzes the effectiveness of the proposed behavioral decision-making algorithm for these three additional scenarios.

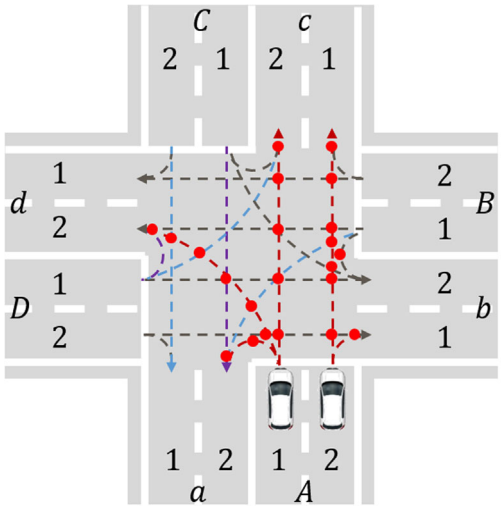

FIGURE 12 Conflict paths of subject vehicle at a standard two-lane intersection

The cost function maps of scenarios 7–9 are shown in Figure 13a–c, respectively. Similarly, the changing trend of the value of the cost function, S, is generally consistent with the six conflict scenarios at an unprotected T-intersection. The results show that the cost function can be used not only in situations where the other vehicles are driving at T-intersections, but also in cases where they are driving at standard multilane intersections. In general, the greater the value of the cost function S is, the higher the risk degree of the traffic scenario is. However, the results are quite different from the previous six scenarios, and the main difference is in the right-hand side of the cost function map. As shown in Figure 13d–f, the number of times the subject vehicle selects to pass in this range increases. This is because each entrance has two lanes in these three scenarios (scenarios 7–9) as in the previous six scenarios, and there are no other vehicles driving straight from the left to the right. Therefore, the subject vehicle has the opportunity to start slowly and wait for other vehicles to cross the intersection before accelerating to complete the left turn.

In scenario 7, the subject vehicle passes the standard two-lane intersection successfully in most of the instances

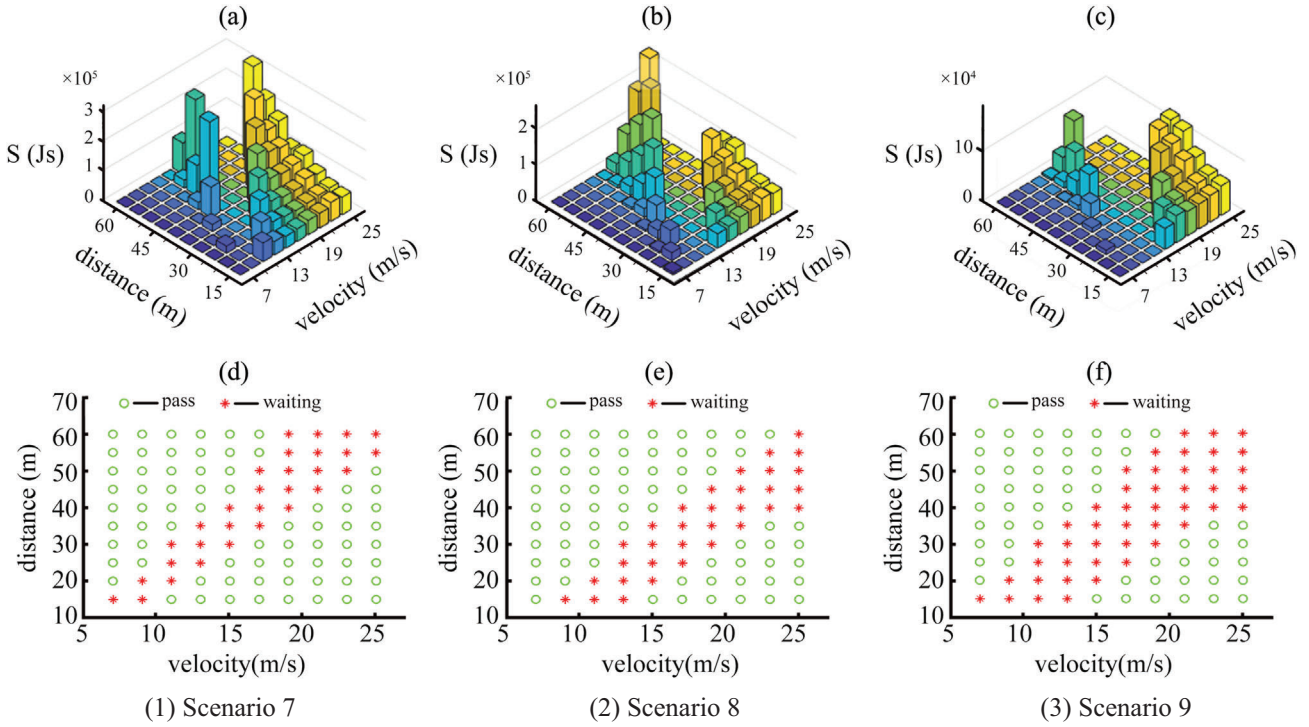

FIGURE 13 Simulation results (scenarios 7–9)

(70 cases). The TTI value of the vast majority of the waiting scenarios is between 1.9 and 2.9 s. In scenario 8, the subject vehicle passes the standard two-lane intersection successfully in two-thirds of the instances (68 cases). The TTI value of the vast majority of the waiting scenarios is between 1.3 and 2.6 s. Finally, in the last scenario, that is, scenario 9, the subject vehicle passes the standard two-lane intersection successfully in more than half of the instances (55 cases). The TTI value of the vast majority of the waiting scenarios is between 1.3 and 3 s.

In addition, the value of the cost function, S, is time-varying with the speed and relative distance of the other vehicle based on the cost function map. This phenomenon is the same as the previous six scenarios. The pass rates from scenarios 7 to 9 are 70%, 68%, and 55%, respectively. It is worth noting that this method still did not cause any collision accidents at a standard multilane intersection.

Similar to the previous section, we utilized the TTI threshold to conduct a total of 2,700 rounds of simulation in these three scenarios under the same simulation conditions. Figure 14 shows the simulation results. Similarly, we set the simulation situation based on different TTI thresholds from 1 to 9 s. As shown in Figure 14, each situation was simulated for 100 rounds. The pass rate can also reach an extremely high value if the TTI threshold is less than 2 s in all the three scenarios. The maximum pass rates in scenarios 7–9 are 68%, 66%, and 52%, respectively. Also, higher pass rates are accompanied by higher collision rates, that is, the smaller the TTI threshold is, the more successful the pass cases as well as collisions will be. Hence, TTI thresholds need to be raised

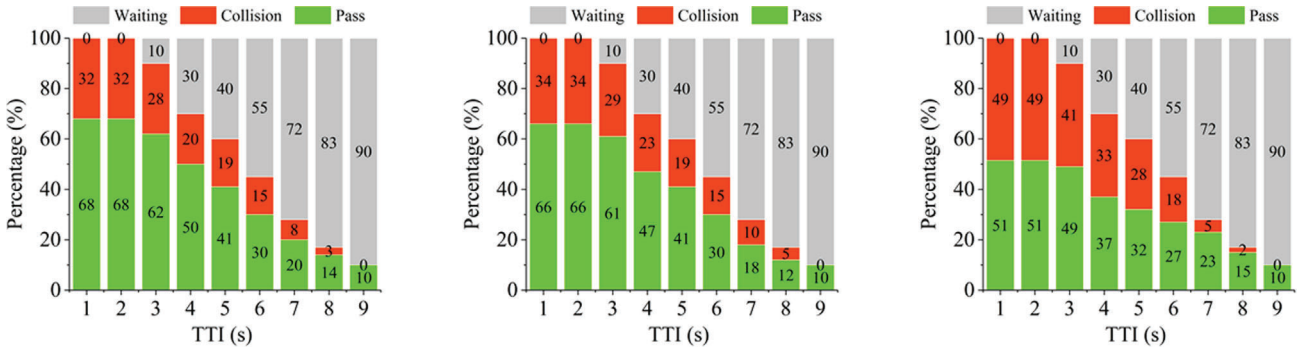

FIGURE 14 Simulation results of TTI thresholds

to improve driving safety. As TTI increases, the collision rate decreases, whereas the number of waiting cases increases and the traffic efficiency decreases. Simulation results of the algorithm at the standard intersection based on TTI threshold show that the same shortcomings of this algorithm are exposed in the simulation of both T-intersections and standard intersections. However, a comparison of the behavioral decision-making model with the TTI threshold method reveals that the former can always avoid collision accidents on the premise of ensuring certain efficiency, and it can achieve 102.94%, 103.03%, and 105.77% of TTI's maximum pass rate in scenarios 7–9, respectively. The results show that the proposed method can also be used in a standard multilane intersection, and also indicate that the TTI threshold approach is less effective in more complex scenarios.

7 | DISCUSSIONS

The intersection is a typical structure of the road traffic environment. Traffic managers usually install traffic lights at the junction of two roads with high-density traffic flows to ensure traffic safety and high travel efficiency. However, traffic lights are not installed for some intersections with low-density traffic flows or with primary and secondary roads to save the installation cost of infrastructure and to reduce the burden of traffic management. Generally, vehicles drive based on the signals of traffic lights at signalized intersections. At unprotected intersections, it is necessary to distinguish two situations: (a) vehicles follow the first-come-first-served rule if intersecting roads have the same priority; (b) otherwise, vehicles need to follow the priorities of their roads. At unprotected intersections, even human drivers often make mistakes that lead to accidents. A recent study found that accidents at unprotected intersections are worse than those at signalized intersections. Moreover, advanced driver assistance technologies, such as AEB systems, will not help mitigate accidents at unprotected intersections (Zhao, Zheng, Wang, Xu, & Kodaka, in press).

Just like human drivers, it is not tricky for intelligent vehicles to follow the signals from traffic lights to cross intersections. However, intelligent vehicles have suffered numerous setbacks at unprotected intersections, especially at unprotected T-intersections, such as the well-known collision between Tesla model 3 and a truck (X. Wang, Zhao, Peng, & LeBlanc, 2017), and the case of Waymo's difficulty in turning left at unprotected T-intersections (Felton, 2018). It is difficult for intelligent vehicles to accurately identify the behavior of other road users in this situation. With the development of V2X technologies, researchers have started to use V2X technologies to replace traffic lights and to explore new management approaches to improve traffic safety and efficiency at intersections (Grembek, Kurzhanskiy, Medury, Varaiya, & Yu, 2019; Xu et al., 2018). In the Grand Cooperative Driving Challenge 2016, the urban test scenario focused on the cooperative crossing of a T-intersection without traffic lights. In the cooperative, separate automated maneuvering protocols were specially designed for unprotected T-intersections (Ploeg et al., 2018). There is no doubt that the current problems faced by intelligent vehicles will be effectively alleviated in a connected vehicle traffic environment in the future. However, V2X technologies are constrained by infrastructure, and it will take a long time to promote these technologies. Therefore, the problem of making safe left turns at unprotected T-intersections is still challenging with the current condition of technology.

8 | CONCLUSIONS

This paper analyzed the factors that affect driving risk and its mechanism. Based on the analysis of the relationship between driving risk and the existing spring models, we presented a vehicle interactions model to describe the driving risk between vehicles clearly. Additionally, we showed that it is feasible and appropriate to apply elastic force and potential energy to estimate driving risk. Furthermore, based on the principle of least action, we proposed a new driving decision-making modeling method by choosing safety and high efficiency as the multiobjective of the decision making of intelligent vehicles. The main results of this study are summarized below:

1. The proposed combined spring model can be used for assessing driving risk, which involves two components: a multispring model with an elliptic distribution and a spring vibrator model between the ellipse foci. The second component of the model uses the elastic force and potential energy to achieve the quantitative evaluation of the vehicle's driving risk based on various attributes (mass) and motion states (speed, acceleration, and relative distance).
2. We introduced a behavioral decision-making model, which could integrate drivers' multiobjective fundamentally based on the principle of least action. Furthermore, we introduced a mechanical system to describe the driving process. We choose safety and high efficiency as the multiobjectives of decision making while driving and the action of the driving process. Moreover, the behavioral decision-making cost function is established from the perspective of the mechanical system. This method provides a new idea for developing a behavioral decision-making algorithm of intelligent vehicles.
3. We designed a typical driving scenario for verifying the simulation experiments of the proposed behavioral decision-making model. The simulation results validated

the effectiveness of the proposed behavioral decision-making model and illustrated that the vehicle control algorithm based on the proposed behavioral decision-making model could solve the technical problems inherent in the Waymo vehicles as observed at the T-intersection and the standard multilane intersection.

Compared with a conventional behavioral decision-making method, the proposed model, which is based on the principle of least action, comprehensively considered safety and high efficiency. In addition, the proposed model is not limited to specific scenarios, such as car following and lane changing. Moreover, it can be applied to arbitrary scenarios and also provides a new way for developing decision-making algorithm of intelligent vehicles.

Future research in this direction involves the following two aspects. The first is on the modeling and evaluation of the combined spring model by considering the lateral acceleration and angular acceleration to describe the driving risk more precisely. We will also improve the model by considering the randomness and uncertainty of the behavior of other drivers. The second is on field experiment design and verification. Moreover, the simulation experiments will focus on how to apply the algorithm to various driving scenarios in real traffic environments.

ACKNOWLEDGMENTS

This work was supported by the National Science Fund for Distinguished Young Scholars (51625503) and the National Natural Science Foundation of China, the Major Project (61790561). We thank Prof. Daiheng Ni for his valuable comments, discussion, and language expression improvement; further, we appreciate Dr. Yougang Bian for his detailed suggestions.

REFERENCES

Bojarski, M., Del Testa, D., Dworakowski, D., Firner, B., Flepp, B., Goyal, P., … Zhang, J. (2016). *End to end learning for self-driving cars*. *arXiv preprint arXiv:1604.07316, 2016*.

Chai, R. (2016). *Research on driving behavior characteristics based on Internet of Vehicles (PhD thesis)*. Beijing Institute of Technology.

Coopersmith, J. (2017). *The lazy universe: An introduction to the principle of least action*. Corby: Oxford University Press.

Dovgan, E., Javorski, M., Tušar, T., Gams, M., & Filipič, B. (2014). Discovering driving strategies with a multiobjective optimization algorithm. *Applied Soft Computing*, *16*, 50–62. https://doi.org/10.1016/j.asoc.2013.11.014

Elgharbawy, M., Schwarzhaupt, A., Frey, M., & Gauterin, F. (2017). A real-time multisensor fusion verification framework for advanced driver assistance systems. *Transportation Research Part F: Traffic Psychology and Behaviour*, *61*, 259–267. https://doi.org/10.1016/j.trf.2016.12.002

Felton, R. (2018). *Google's self-driving cars have trouble with basic driving tasks: Report*. Jalopnik. Retrieved from https://jalopnik.com/googles-self-driving-cars-have-trouble-with-basic-drivi-1828653280

Fu, G. (2013). *Safety management—A behavior-based approach to accident prevention*. Beijing: Science Press.

Green M. (2000). How long does it take to stop? Methodological analysis of driver perception-brake times. *Transportation Human Factors*, *2*(3), 195–216.

Grembek, O., Kurzhanskiy, A., Medury, A., Varaiya, P., & Yu, M. (2019). Making intersections safer with I2V communication. *Transportation Research Part C: Emerging Technologies*, *102*, 396–410. https://doi.org/10.1016/j.trc.2019.02.017

Gu, T., & Dolan, J. M. (2014). *Toward human-like motion planning in urban environments*. Intelligent Vehicles Symposium Proceedings, IEEE, 350–355.

Hammer, W. (1972). *Handbook of system and product safety*. Englewood Cliffs, NJ: Prentice-Hall.

Hammer, W. (2003). *Occupational safety management and engineering (5th ed). Prentice-Hall International Series in Industrial and Systems Engineering*. Beijing: Tsinghua University Press.

Helbing, D., & Tilch, B. (1998). Generalized force model of traffic dynamics. *Physical Review E*, *58*, 133.

Hoult, W., & Cole, D. J. (2008). A neuromuscular model featuring co-activation for use in driver simulation. *Vehicle System Dynamics*, *46*, 175–189.

Jo, K., Kim, J., Kim, D., Jang, C., & Sunwoo, M. (2015). Development of autonomous car—Part II: A case study on the implementation of an autonomous driving system based on distributed architecture. *IEEE Transactions on Industrial Electronics*, *62*, 5119–5132.

Landau, L. D., & Lifshitz, E. M. (2013). *Course of theoretical physics*. Oxford: Elsevier.

Li, S., Li, K., Rajamani, R., & Wang, J. (2011). Model predictive multi-objective vehicular adaptive cruise control. *IEEE Transactions on Control Systems Technology*, *19*, 556–566. https://doi.org/10.1109/TCST.2010.2049203

Lin, D., Ma, W., Li, L., & Wang, Y. (2016). A driving force model for non-strict priority crossing behaviors of right-turn drivers. *Transportation Research Part B: Methodological*, *83*, 230–244. https://doi.org/10.1016/j.trb.2015.10.007

Mohanan, M. G., & Salgoankar, A. (2018). A survey of robotic motion planning in dynamic environments. *Robotics and Autonomous Systems*, *100*, 171–185.

Nolte, M., Ernst, S., Richelmann, J., & Maurer, M. (2018). *Representing the unkown-impact of uncertainty on the interaction between decision making and trajectory generation*. 21st International Conference on Intelligent Transportation Systems (ITSC). IEEE, 2018, 2412–2418.

Okuda, H., Ikami, N., Suzuki, T., Tazaki, Y., & Takeda, K. (2013). Modeling and analysis of driving behavior based on a probability-weighted ARX model. *IEEE Transactions on Intelligent Transportation Systems*, *14*, 98–112.

Ploeg, J., Semsar-Kazerooni, E., Medina, A. I. M., de Jongh, J. F. C.M., van de Sluis, J., Voronov, A., … van de Wouw, N. (2018). Cooperative automated maneuvering at the 2016 grand cooperative driving challenge. *IEEE Transactions on Intelligent Transportation Systems*, *19*, 1213–1226. https://doi.org/10.1109/TITS.2017.2765669

Raksincharoensak, P., Akamatsu, Y., Moro, K., & Nagai, M. (2014). Driver speed control modeling for predictive braking assistance system based on risk potential in intersections. *Journal of Robotics and Mechatronics*, *26*, 628–637. https://doi.org/10.20965/jrm.2014.p0628

Sun, D.J., & Elefteriadou, L. (2012). Lane-changing behavior on urban streets: An "In-Vehicle" field experiment-based study. *Computer-Aided Civil and Infrastructure Engineering*, *27*, 525–542. https://doi.org/10.1111/j.1467-8667.2011.00747.x

Teichman, A., Lussier, J. T., & Thrun, S. (2013). Learning to segment and track in RGBD. *IEEE Transactions on Automation Science and Engineering*, *10*, 841–852.

Wang, J., Wu, J., & Li, Y. (2015). The driving safety field based on driver–vehicle–road interactions. *IEEE Transactions on Intelligent Transportation Systems*, *16*, 2303–2314.

Wang, X., Zhao, D., Peng, H., & LeBlanc, D. J. (2017). *Analysis of unprotected intersection left-turn conflicts based on naturalistic driving data*. Presented at the 2017 IEEE Intelligent Vehicles Symposium (IV), 218–223.

Wang, Z., Chen, X., Ouyang, Y., & Li, M. (2015). Emission mitigation via longitudinal control of intelligent vehicles in a congested platoon. *Computer-Aided Civil and Infrastructure Engineering*, *30*(6), 490–506. https://doi.org/10.1111/mice.12130

Wei, J., Snider, J. M., Gu, T., Dolan, J. M., & Litkouhi, B. (2014). *A behavioral planning framework for autonomous driving*. 2014 IEEE Intelligent Vehicles Symposium Proceedings, IEEE, 458–464.

Xu, B., Li, S. E., Bian, Y., Li, S., Ban, X. J., Wang, J., & Li, K. (2018). Distributed conflict-free cooperation for multiple connected vehicles at unsignalized intersections. *Transportation Research Part C: Emerging Technologies*, *93*, 322–334. https://doi.org/10.1016/j.trc.2018.06.004

Zhao, Z., Zheng, X., Wang, J., Xu, Q., & Kodaka, K. (in press). Assessing the performance of the collision mitigation brake system in the Chinese traffic environment. *Journal of Central South University*. https://www.researchgate.net/publication/334587026_Assessing_the_Performance_of_the_Collision_Mitigation_Brake_System_in_the_Chinese_Traffic_Environment

Zheng, X., Zhang, D., Gao, H., Zhao, Z., Huang, H., & Wang, J. (2018). A novel framework for road traffic risk assessment with HMM-based prediction model. *Sensors*, *18*, 4313. https://doi.org/10.3390/s18124313

Zhu, F., & Ukkusuri, S. V. (2018). Modeling the proactive driving behavior of connected vehicles: A cell-based simulation approach. *Computer-Aided Civil and Infrastructure Engineering*, *33*, 262–281. https://doi.org/10.1111/mice.12289

How to cite this article: Zheng X, Huang H, Wang J, Zhao X, Xu Q. Behavioral decision-making model of the intelligent vehicle based on driving risk assessment. *Comput Aided Civ Inf*. 2019;1–18. https://doi.org/10.1111/mice.12507